Instabilities of charged polyampholytes

Yacov Kantor
Department of Physics, Massachusetts Institute of Technology, Cambridge, Massachusetts 02139;
Physics Department, Harvard University, Cambridge, Massachusetts 02138;
*School of Physics and Astronomy, Tel Aviv University, Tel Aviv 69 978, Israel**

Mehran Kardar
Department of Physics, Massachusetts Institute of Technology, Cambridge, Massachusetts 02139
(Received 24 August 1994)

We consider polymers formed from a (quenched) random sequence of charged monomers of opposite signs. Such polymers, known as polyampholytes (PA's), are compact when completely neutral and expanded when highly charged. We examine the transition between the two regimes by Monte Carlo simulations, and by analogies to charged drops. We find that the overall excess charge Q is the main determinant of the size of the PA's. A polymer composed of N charges of $\pm q_0$ is compact for $Q < Q_c \approx q_0\sqrt{N}$ and expanded otherwise. The transition is reminiscent of the Rayleigh shape instability of a charged drop. A uniform excess charge causes the breakup of a fluid drop. We speculate that a uniformly charged polymer stretches out to a *necklace* shape. The inhomogeneities in charge distort the shape away from an ordered necklace.

PACS number(s): 36.20.−r, 33.15.Bh, 64.60.−i, 41.20.−q

I. INTRODUCTION

Polyampholytes (PA's) are long chain macromolecules with a random mixture of oppositely charged groups fixed along their backbone [1]. Several elements conspire to make the behavior of such heteropolymers a problem of great interest. One (admittedly somewhat remote) motivation is the similarity to the macromolecules of biological interest such as nucleic or amino acids. The specific sequence of monomers on such chains is essential to biological activity. For example, the sequence of amino acids determines the ultimate shape of a protein [2]. Attempting to unravel the precise factors responsible for *protein folding*, several statistical models have been proposed [3]. These models sacrifice the specificity of particular proteins, by essentially focusing on generic properties of heteropolymers with competing interactions [4]. PA's can be regarded as a particular example of this class. From another perspective, properties of random systems with competing interactions have been on the forefront of statistical mechanics for the past decade [5]. The prototype of complexity in this class of problem, the spin glass, has much in common with random heteropolymers. The statistics of the ground state, and those of low lying excitations, is paramount to both systems. As examples of *soft* condensed matter, heteropolymers have the advantage of faster relaxation, compared to their "harder" counterparts. Indeed there is much encouragement from recent experimental studies of solutions [6] and gels composed of PA's [7,8].

It may appear that the long-range nature of the Coulomb interaction between charges is yet an additional complication of an already hard problem. Yet for a uniformly charged polymer (a polyelectrolyte), it is possible to find the *exact* scaling of the radius of gyration R_g on the number of monomers N [9]. The proof relies on the nonrenormalization of the dimensionless interaction parameter $u = Q^2/(k_BTR_g^{d-2})$ in d embedding dimensions. Since $Q \propto N$, it follows that $R_g \sim N^\nu$, with $\nu = \nu_h \equiv 2/(d-2)$ (for $4 \leq d \leq 6$). Inspired by the simplicity of the homogeneous case, we suggested a similar argument for the randomly charged PA [10]. Consider a model PA composed of N charges $\pm q_0$, randomly and independently chosen at each site. Although the mean net charge is zero, a typical PA has excess charge of order $\pm q_0\sqrt{N}$. Independent of its sign, this leads to a repulsive self-energy, on average described by the dimensionless parameter $\overline{u} = Nq_0^2/(k_BTR_g^{d-2})$. Assuming that this parameter is not renormalized as in the uniformly charged case leads to a swelling exponent of $\nu = 1/(d-2)$ (for $3 \leq d \leq 4$), i.e., a polymer that is *stretched* in $d = 3$.

However, in an electrolytic solution oppositely charged ions rearrange so as to screen the long-range Coulomb interaction. The net effect is an attractive energy [11], described by the Debye-Hückel (DH) theory. Higgs and Joanny [12] assumed that the monomers in a PA can similarly rearrange to *compact* configurations, thereby taking advantage of the DH attraction. A partial resolution of the contradiction between the two predictions is obtained by noting that DH theory requires the exact neutrality of the electrolyte, while the renormalization-group-(RG) inspired approach depends on the excess charge in a typical sequence. Monte Carlo simulations [13,14] indeed confirm that PA's with $Q = 0$ become compact at low temperatures. By contrast, sampling all random

*Permanent address.

quenches with unrestricted Q produces a broad range of sizes, with an average consistent with $\overline{R_g} \propto N$.

Depending on the conditions, experiments observe both compact and expanded conformations [6]. One set of experiments [7] was performed on gels produced by crosslinking PA's [8]. By changing the conditions of the solvent (pH, salt content, etc.), it is possible to control both the excess charge Q on the PA chains and the screening length. Due to the large screening length, the Coulomb interactions are significant. As a function of Q, the gel undergoes dramatic changes in volume, the neutral gel being the most compact. However, the volume of the gel does not change gradually with increasing charge. There is an interval of Q around the neutral point where the gel remains compact, suddenly increasing in volume by an order of magnitude beyond a threshold Q_c. The threshold scales with the number of monomers N, within a screening length, as $Q_c \approx q_0\sqrt{N}$. Motivated by the experimental results, we undertook a systematic examination of the dependence of the size of a PA on its excess charge. Monte Carlo simulations show that PA's are compact for small Q, and expanded when Q exceeds a critical value of $Q_c \approx q_0\sqrt{N}$, in complete analogy with the experiments. Some aspects of this transition can be understood by analogy to the behavior of a charged drop. The spherical drop is stable for charges smaller than a Rayleigh limit $Q_R \propto \sqrt{V}$, where V is the volume of the drop. Charged beyond this point, the drop elongates to minimize the Coulomb repulsion. The elongated drop rapidly disintegrates into smaller droplets. In attempting to follow a similar scenario, a PA chain breaks into a necklace of globules connected by strings. The detailed shape of the necklace is determined by charge inhomogeneities.

The main results of this work were summarized in an earlier publication [15]. Here we provide more detailed results and additional information. The paper is organized as follows. The competing arguments applied to PA's are discussed in some detail in Sec. II, and their inconsistencies are emphasized. The results of Monte Carlo simulations on the dependence of the radius of gyration of the polymer on temperature and excess charge are presented in Sec. III. Various details of the Monte Carlo procedure are relegated to Appendix A. We argue that as Q is increased beyond a threshold Q_c, the PA undergoes a sudden transition from a compact to a strongly elongated state. In Sec. IV we provide a qualitative picture of this transition by analogy to the shape instability of a charged drop. Some known results pertaining to such drops, as well as new calculations for spheroidal shapes, are presented in Appendix B. Such analogies cannot be extended to the strongly distorted limit where, as argued in Sec. V, a uniformly charged polymer deforms into a necklace of compact beads. Such a shape is the best compromise for the PA in trying to mimic the ground state of a charged drop, which, as described in Appendix C, is obtained by splitting into several droplets. In Sec. VI we point out the importance of quenched randomness in the PA. An ordered necklace is not stable to charge inhomogeneities, and the beads must rearrange in complicated shapes dependent on the details of randomness.

II. POLYAMPHOLYTE PHENOMENOLOGY

In this work we consider PA's immersed in a good solvent in which the concentration of counterions is small, and hence the electrostatic interactions are treated as unscreened. Experimentally, the details of a charge sequence are determined by its fabrication process. *Markovian* sequences are constructed by adding one monomer at a time, the probability of choosing a particular monomer (e.g., positively or negatively charged) depends only on the last monomer [16]. Such a construction leads to correlations in the charges q_i, which decay exponentially as

$$\overline{q_i q_j} = q_0^2 \lambda^{|i-j|}, \quad -1 < \lambda < 1. \tag{1}$$

The extreme limits of $\lambda = -1$ and $\lambda = 1$ correspond to *nonrandom* sequences that are alternating [17], or fully charged, and will not be considered here. The behavior for λ is asymptotically similar to the case where the charges are uncorrelated ($\lambda = 0$), and we shall focus mostly on such chains.

We shall, however, allow for the possibility that the total charge of the chain is constrained to a particular value of Q. Experimentally, this net charge can be controlled by changing the pH, and other properties of the solvent. At several points we shall also contrast the behavior of *quenched* and *annealed* PA's; the latter is defined as a predetermined collection of positive and negative charges which can freely move along the polymer chain. Note that in this definition the total charge is fixed. If this constraint is also removed the polymer lowers its energy by getting rid of any excess charge. Note that such annealed PA's are not very realistic, and should not be confused with the case considered by Raphael and Joanny [18], where the excess charge can adjust its value depending on the temperature, concentration of PA's, and concentration of the counterions.

A short ℓ-monomer segment of a PA with uncorrelated random monomers has typical charge of $q_0\sqrt{\ell}$. If we assume that the segment is a self-avoiding walk, its radius of gyration is approximately $a\ell^\nu$, where a is a microscopic length (e.g., the monomer diameter or nearest neighbor separation along the chain). As the typical electrostatic energy of such a subchain is $q_0^2\ell^{1-\nu}/a$, interactions become important for $T \approx q_0^2\ell^{1-\nu}/a$. (We shall henceforth measure temperature in energy units, i.e., set $k_B = 1$.) Alternatively, we can define $\ell_T = (Ta/q_0^2)^{1/(1-\nu)}$, and divide the entire chain into segments of ℓ_T monomers. The interactions within each segment are small compared with T, while interactions between the segments are strong. Such segments form the basic "ions" in an analogy [19] between PA's and usual electrolytes [11] employed by Higgs and Joanny [12]. The spatial extent of each segment is

$$a_T = a\ell_T^\nu = \begin{cases} a\left(\frac{Ta}{q_0^2}\right)^{\nu/(1-\nu)} & \text{for } T > q_0^2/a \\ a & \text{for } T < q_0^2/a. \end{cases} \tag{2}$$

For the generalized Markovian chains, the net charge of a sufficiently long segment (such that $\lambda^\ell \ll 1$) grows

as $q_0\sqrt{N(1+\lambda)/(1-\lambda)}$. The previous argument thus remains valid after replacing q_0 by $q_0\sqrt{(1+\lambda)/(1-\lambda)}$. This simple change is sufficient to relate most high-temperature properties of the short-range correlated sequences to the uncorrelated ones (e.g., in a high-temperature series expansion for the radius).

In the spirit of a RG analysis, we can attempt to increase the short distance cutoff along the sequence by a factor ℓ. Perturbations around the high-temperature phase depend on the *dimensionless* interaction parameter $u \equiv q_\ell^2/r_l T \ll 1$, where q_ℓ is a typical charge on length scale ℓ, while r_ℓ is the spatial extent of the shortest segments. Upon rescaling the cutoff by a factor b, q_ℓ increases by $\sqrt{b}$, while r_ℓ scales by b^ν, as in a self-avoiding walk. Thus the renormalized interaction parameter $u(b) = b^{1-\nu}u$ grows under rescaling and reaches unity for ℓ equal to ℓ_T defined above. At this scale r_ℓ becomes of the same order as a_T. Beyond this point the interactions are *relevant*, strongly modifying the behavior of the chain.

Different approaches to the problem are in agreement in the weak coupling regime of $u \ll 1$. The strong coupling regime is not easily tractable, and different assumptions lead to different conclusions. Higgs and Joanny [12] construct the free energy of a long PA by first assuming that it has a uniform density and then proving this assumption self-consistently. (See also Refs. [13,14].) In this approach the N-monomer PA is divided into blobs [20] of ℓ_T monomers each, forming a liquid of uniform density as depicted qualitatively in Fig. 1(a). The blobs are noninterpenetrating and arranged so that the neighborhood of each blob is predominantly occupied by blobs of opposite charge. This arrangement roughly resembles the structure of a salt crystal. The excess charge of each blob is effectively screened and the dense configurations take energetic advantage of the large number of neighbors of opposite sign. The energy gain per blob is approximately the nearest neighbor interaction, i.e., $\epsilon_c(T) \approx q_0^2\ell_T/a_T$. We note, however, that even in the ideal NaCl crystal, the condensation energy per atom ($0.874q_0^2/a$) is a small fraction of the interaction energy between the nearest neighbors ($3q_0^2/a$), and is thus strongly influenced by further neighbors. The validity of the picture depicted in Fig. 1(a) rests on the assumption that it is possible to fold a randomly charged object in a way that not only provides the correct neighborhood to each charge, but also keeps more extended neighborhoods approximately neutral. Thus such configurations require the possibility of specific foldings of the PA at both local and global levels.

The primary focus of the DH-type approach is the minimization of the extensive part of the energy by creating a homogeneous liquidlike structure, while nonextensive energies due to surface tension and electrostatics are relegated the role of determining the overall shape of the globule. By contrast, a RG-inspired approach [10] to the problem assumes that the blobs form a *self-similar* structure [as depicted in Fig. 1(b)] which attempts to take care of energies on every length scale. In d space dimensions, the dimensionless interaction parameter at scale ℓ is $u(\ell) = q_0^2\ell/(Tr_\ell^{d-2})$. This expression represents the typical interaction energy of a random ℓ-monomer segment, *assuming* that the Coulomb interactions cannot be screened. For a self-similar structure with $r_\ell \propto \ell^{\nu'}$, $u(\ell) \propto \ell^{1-(d-2)\nu'}$, and the interaction parameter grows or diminishes under rescaling unless $\nu' = 1/(d-2)$. [The analogous argument leads to the exact value of $\nu_h = 2/(d-2)$ for uniform polyelectrolytes where no screening is possible [20].] This result is valid only for

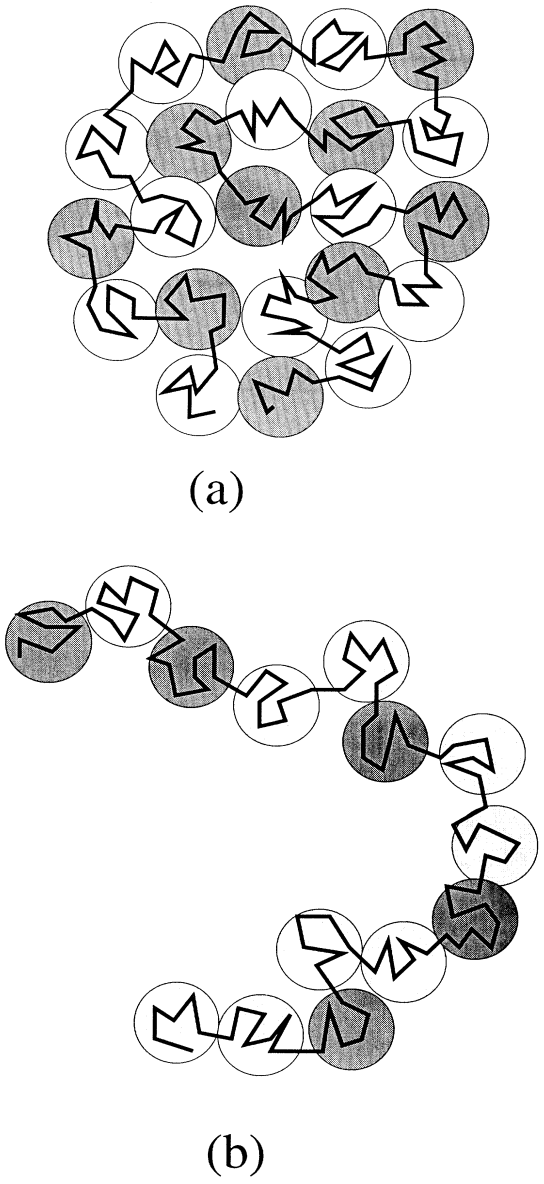

FIG. 1. Qualitative views of the spatial arrangement of "blobs" in a PA with quenched randomness. Electrostatic interactions within each blob are smaller than k_BT. Lighter and darker shades of the spheres denote predominantly positively or negatively charged blobs. The DH view assumes that the blobs can rearrange in a pattern (a) where interactions are screened on long distances. According to a RG-inspired picture the blobs form a self-similar pattern (b) with the same interaction energy on all length scales.

$3 \leq d \leq 4$: For $d > 4$ the electrostatic interactions are irrelevant and $\nu = 1/2$, while for $d < 3$ the polymer is stretched ($\nu' = 1$). Keeping interactions equally strong on all length scales also generates a condensation energy proportional to Nq_0^2/a. However, as this argument does not provide the prefactor, i.e., the actual value of the condensation energy, it is not possible to deduce whether the DH-type or RG-type ansatz produces the lower free energy state.

Are the two aforementioned approaches mutually exclusive? In this work we present evidence that they actually represent two facets of the same problem: DH theory attempts to minimize the condensation energy without paying attention to the surface. However, an object can be (locally) "compact" and still have an extremely extended shape which is controlled by the nonextensive part of the energy. The RG-inspired approach attempts to accommodate the latter energy.

III. NUMERICAL SIMULATIONS

Configurations of a polymer are completely specified by listing the position vectors $\{\mathbf{r}_i\}$ $(i = 1, \ldots, N)$ of its monomers. The shape and spatial extent of the polymer are roughly characterized by the shape tensor,

$$\mathcal{S}_{\mu\nu} = \frac{1}{N}\sum_{i=1}^{N} r_{i\mu} r_{i\nu} - \frac{1}{N^2}\sum_{i=1}^{N} r_{i\mu} \sum_{j=1}^{N} r_{j\nu} \ , \qquad (3)$$

where the greek indices denote the Cartesian components of the vectors. Thermal averages of the ordered eigenvalues $\lambda_1 > \lambda_2 > \lambda_3$ of this tensor (sometimes referred to as moments of inertia) are used to describe the mean size and shape; their sum, i.e., the thermal average of $\mathrm{tr}\mathcal{S}$, is the squared radius of gyration R_g^2. Since we are dealing with sequences of quenched disorder, these quantities must also be averaged over different realizations. In three dimensions, uniform uncharged polymers in good solvents are swollen; their R_g scaling as N^ν with $\nu = 0.588$ as in self-avoiding walks. Polymers in poor solvents are "compact," i.e., described by $\nu = \frac{1}{3}$.

The Monte Carlo procedure used in this work is identical to that described in Ref. [13]. Here we describe some important features, while the more technical details are described in Appendix A. The simulated chains are composed of N monomers whose positions are discretized to a cubic lattice ($d = 3$) with lattice constant a. The connectivity of the polymer is maintained by restricting the maximal distance between neighbors to $4a$. The excluded-volume interaction is enforced by not allowing two monomers to come any closer than $\sqrt{2}a$. Each quench is characterized by a set of charges $q_i = \pm q_0$. The electrostatic interactions between the charges, $\mathcal{U} = \sum_{\langle i,j\rangle} U_{ij}(|\mathbf{r}_i - \mathbf{r}_j|)$, are included by assigning energy $U_{ij}(r) = q_i q_j/\sqrt{c + r^2}$ to each pair $\langle i, j\rangle$ at a separation distance r, with $c = 2a^2$, which "softens" the potential at short distances.

The results of the simulations are parametrized by the chain length N, temperature T, and the overall excess charge $Q = \sum_i q_i$. Each Q can be obtained by many realizations of randomness, and all results were averaged over ten different quenches. However, rather than taking the same configurations through changing temperatures, ten distinct quenches were used for each T and Q. The smoothness in variations of various quantities with temperature then provides added confidence in the thermal and quench averaging process. Not surprisingly, as explained in Appendix A, the overall uncertainties are entirely due to quench averaging as the statistical errors of the thermal averages are smaller than the differences between quenches.

Figure 2 depicts the temperature dependence of R_g^2 for 64-monomer chains. The number near each curve indicates the charge, Q/q_0. At very high temperatures the electrostatic interactions are unimportant and the chains behave as self-avoiding walks, with $R_g \propto N^\nu$ and $\nu = 0.588$. The typical electrostatic energy of such configurations is estimated as

$$\overline{\langle U\rangle} \approx \sum_{i,j} \overline{q_i q_j} \left\langle \frac{1}{|\mathbf{r}_i - \mathbf{r}_j|} \right\rangle \approx \frac{(Q^2 - q_0^2 N)}{R_g}, \qquad (4)$$

where we have employed $\overline{q_i q_j} = (Q^2 - q_0^2 N)/N^2$ for $i \neq j$, and used R_g as a measure of interparticle separation. Note that the interaction changes sign at

$$Q_c = q_0\sqrt{N} \ . \qquad (5)$$

This is because the energy of strongly charged polymers is dominated by the *repulsive* interaction of excess charges. However, for weakly charged polymers, there is an *attractive* interaction between fluctuations in the charge distribution; the typical fluctuation of Q leads to the above result.

As the temperature of the chain is lowered, the effects of interactions become apparent for

$$T_Q \approx \overline{\langle U\rangle} \approx (Q^2 - q_0^2 N)/aN^\nu \ . \qquad (6)$$

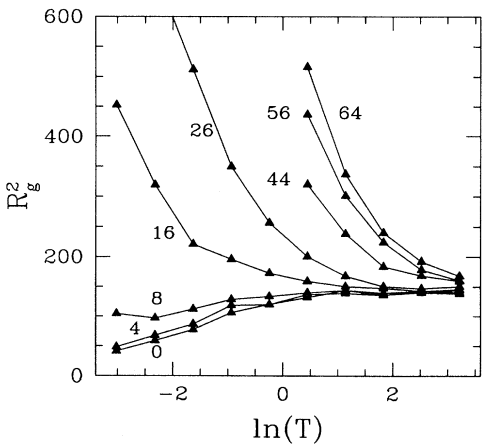

FIG. 2. R_g^2 (in units of a^2) as a function of T (in units of q_0^2/a) for several values of the excess charge Q for a 64-monomer chain. Each point is an average over the ten independent quenches used at each temperature. The numbers near each curve indicate Q/q_0.

Chains with charge larger than Q_c expand, while those with $Q < Q_c$ shrink with decreasing temperature. The strongest deviation occurs for the fully charged polymer, which for $N = 64$ starts at $T_Q \approx 320q_0^2/a$. For $Q = 0$, the deviation begins at the much lower temperature of $T_Q \approx 5q_0^2/a$. Indeed, on the logarithmic scale of Fig. 2 the departure from the infinite temperature values of R_g^2 is most apparent for $Q = 64q_0$, starting at $\ln(T) \approx 6$ (beyond the limits of the figure), compared to $\ln(T) \approx 1.7$ for $Q = 0$.

To see if the *averages* in Fig. 2 provide a good measure of the PA size at low temperatures, we constructed histograms of the distribution of R_g^2 at $T = 0.05q_0^2/a$ for several values of Q. As thermal fluctuations are small, the histograms in Fig. 3 represent differences between quenches. The distributions are fairly narrow, their widths not exceeding the distance between their averages. Thus a point in Fig. 2 provides a good measure of $R_g^2(Q)$, independent of further details of the sequence.

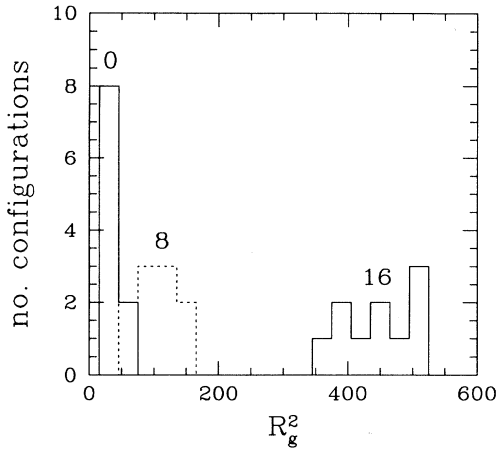

FIG. 3. Histograms of the distribution of the (ten) values of R_g^2 (measured for $N = 64$ at $T = 0.05q_0^2/a$) for several charges Q/q_0, indicated near the histograms.

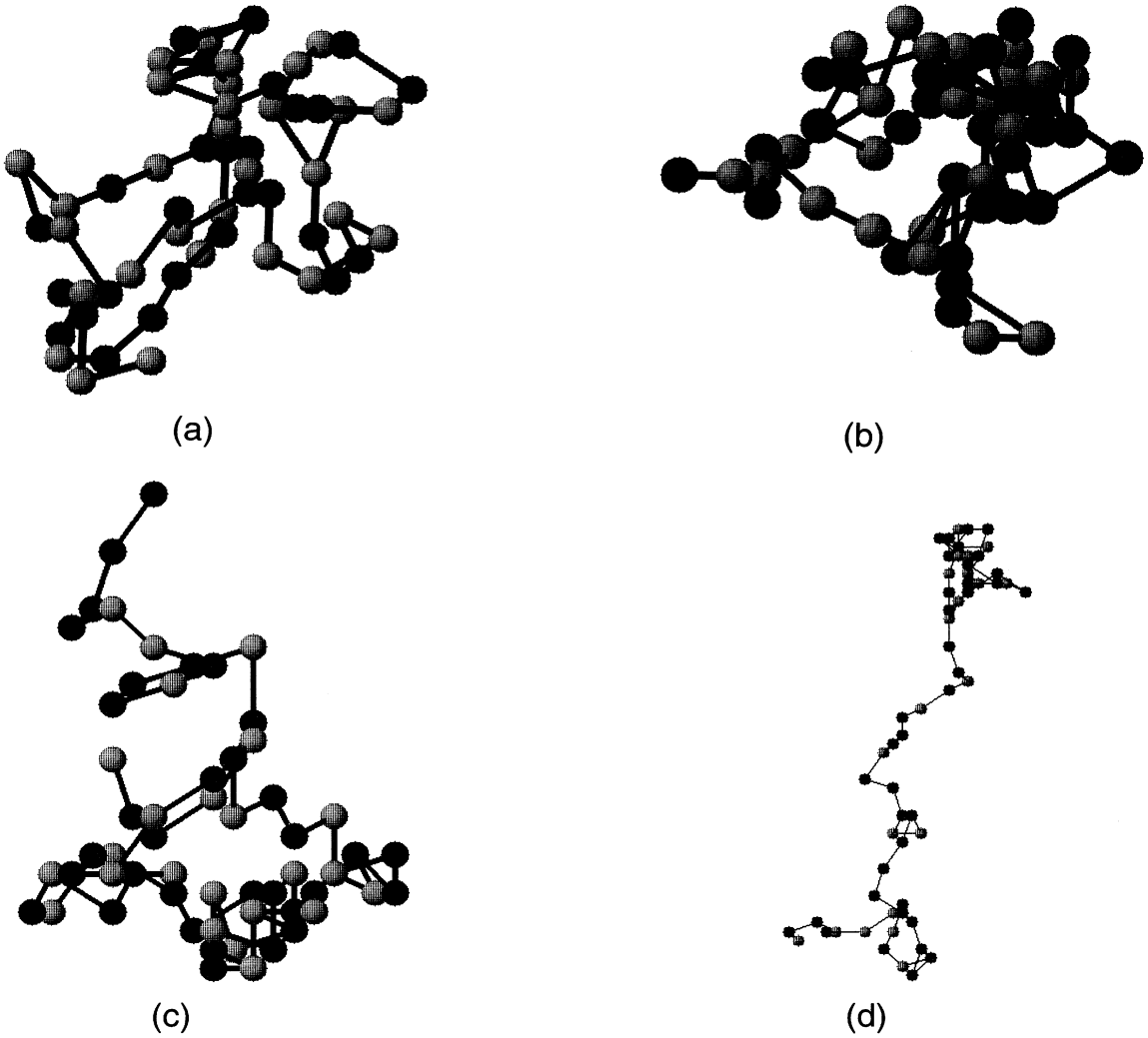

FIG. 4. Spatial conformations of 64-monomer PA's at $T = 0.05q_0^2/a$, for values of Q/q_0 equal to (a) 0, (b) 4, (c) 8, and (d) 16. Dark and bright shades indicate opposite charges. The diameter of each sphere is about 0.4 of the actual excluded-volume range.

The average of R_g^2 for *unrestricted* quenches is then obtained from $R_g^2(Q)$ as

$$R_g^2(\text{random}) = \int_0^\infty dQ R_g^2(Q) P(Q) \ , \tag{7}$$

where $P(Q) \propto \exp[-Q^2/(2q_0^2 N)]$ is the probability density of an excess charge Q. In previous work [13], we found a very broad distribution for R_g^2(random). Even in sampling a few quenches, there were several completely collapsed, and some strongly stretched configurations. Figure 4 shows the spatial conformations of several quenches examined in this study. The weakly charged configurations for $Q/q_0 = 0$ or 4 are spherical globules, indistinguishable from each other. The chains are slightly expanded for $Q/q_0 = 8$, while for $Q/q_0 = 16$, a value of only twice Q_c, they are strongly stretched. It can now be appreciated that the previously observed breadth of the distribution for R_g^2(random) simply follows from the strong dependence of R_g^2 on Q rather than indicating a large scatter of R_g^2 among different quenches with the same Q.

The averaged radii of PA's in Fig. 2 change monotonically with temperature. This suggests that compact and extended states are separated in the (Q,T) plane by a straight line starting from $Q = Q_c = q_0\sqrt{N}$ at infinite T. This hypothesis was tested by looking at the Q and N dependence of the radius of gyration for chains of lengths $N = 16$, 32, 64, 128. To achieve good thermal averages, simulations were performed at $T = 0.1q_0^2/a$ and not at the lowest temperature in Fig. 2. The dependence of R_g^2 on Q is depicted in Fig. 5. The vertical axis is scaled by $N^{2/3}$ to remove the N dependence of the R_g^2 of the compact globules at $Q = 0$. The charges on the horizontal axis are scaled by $Q_c(N)$ for all polymer lengths. Although monotonic, R_g^2 exhibits strong variations with Q. The radius is barely increasing for small Q, but an extremely steep rise begins beyond a threshold charge. Due to the monotonic increase or decrease of PA sizes

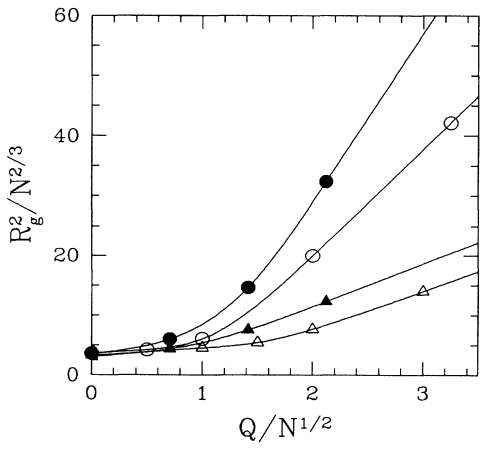

FIG. 5. Scaled R_g^2 as a function of Q/q_0 for chain lengths $N = 16$ (open triangles), 32 (full triangles), 64 (open circles), and 128 (full circles).

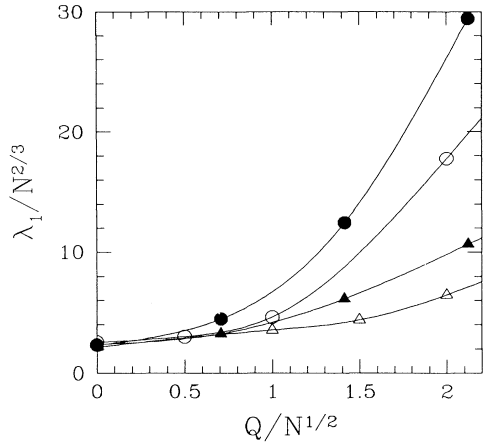

FIG. 6. Scaled largest eigenvalue λ_1 of the shape tensor as a function of charge Q/q_0 for several chain lengths. The symbols are the same as in Fig. 5.

with temperature, this variation becomes even sharper at low temperatures. Figure 5 strongly suggests that the transition from compact to stretched configurations at low temperatures still occurs for $Q \approx Q_c$.

When the distortions of a globular object are small, the changes in R_g^2 are not very sensitive to the changes in shape. The increase in the largest eigenvalue of the shape tensor λ_1 due to elongation of the object is partially compensated by a decrease of other eigenvalues. Figure 6 is analogous to Fig. 5 except that it depicts the charge dependence of the λ_1. The strong elongation of the PA for $Q > Q_c$ is also apparent from this figure.

IV. ANALOGIES TO CHARGED DROPS

To explain the above results, we start with the empirical observation that PA's with vanishing excess charge Q compact to spherical "globules" of spatial extent $R \approx aN^{1/3}$ and surface area $S \approx a^2N^{2/3}$. It is thus natural to represent the total energy (or rather the quench-averaged free energy) of such globules as a sum of condensation and surface energies,

$$E_{\text{PA}}(Q = 0) = -\epsilon_c N + \gamma S \ . \tag{8}$$

The condensation energy is proportional to q_0^2/a, while the surface tension is $\gamma = pq_0^2/a^3$, where the dimensionless prefactor $p \approx 0.1$ is found to be rather small [21]. It should be emphasized that Eq. (8) *is not self-evident* as it represents the average energy of a *connected* chain of N monomers with long-range interactions, rather than N independent particles. While the existence of an extensive condensation energy is natural, nonextensive corrections may in principle be present without any relation to the surface. The presence of the surface term is deduced from the numerical observations that the object is approximately spherical. We may hope that this form of the energy persists as long as the deformations of the globule are not too large.

If we now uniformly add a very small number ($Q/q_0 \ll N^{1/3}$) of charges along the chain (e.g., by randomly replacing $Q/2q_0$ of negative charges by positive ones), without modifying the spatial conformation of the PA, its total energy increases approximately by $q_0|Q|/a$, representing the sum of changes in *local* interactions. For moderate charges ($Q > q_0 N^{1/3}$) the energy increase is dominated by the long-range interactions and is of order Q^2/R. If the PA is now allowed to relax, it will lower its energy by finding more favorable configurations, and thus,

$$E_{\rm PA}(Q) \leq -\epsilon_c N + \gamma S + Q^2/R \ . \tag{9}$$

The above considerations are equally applicable to a charged drop, and we shall explore such analogies to treat weakly distorted PA's. In the following paragraphs, we initially review the results pertaining to the shape of a charged *conducting* drop. This analogy is most appropriate for an annealed version of the problem in which the charges are free to move along the polymer chain. We then go on to consider the shape of a charged *insulating* drop of immobile charges, which is a better representation of quenched PA's.

For a *conducting* drop all the charge accumulates on the surface. The nonextensive contribution to the energy of a freely suspended spherical drop of radius R is

$$E(Q) = \frac{1}{2}\frac{Q^2}{R} + 4\pi R^2\gamma \ . \tag{10}$$

However, the drop can change shape to minimize the sum of surface tension and Coulomb energies. The surface energy of an uncharged drop, $E(0) = 4\pi R^2\gamma$, sets the overall energy scale of the problem while the dimensionless parameter,

$$\alpha \equiv Q^2/(16\pi R^3\gamma) \equiv Q^2/Q_R^2 \ , \tag{11}$$

determines its shape. We shall refer to Q_R as the Rayleigh charge of the drop. Note that the estimates of γ and R following Eq. (8) for the model PA lead to $Q_R \approx Q_c$. Let us initially consider only small deformations in shape of a single drop. Investigations of the shape of charged liquid drops go back at least to the last century [22]. Some of the several variants of this problem are (a) a freely suspended charged conducting drop [22–27]; (b) an uncharged conducting drop in an external electric field [28,29]; (c) a dielectric drop embedded in a different dielectric liquid in an external electric field [30–34]. The last problem has received recent attention because it is mathematically identical to that of a drop of magnetic fluid in a magnetic field [32,34–37]. The conducting drop is the limiting case of an insulating drop with infinite dielectric constant. Problems (a) and (b) are strongly related since similar shape instabilities are induced by both the external field and the internally generated field of a charged drop. In fact, in many experimental situations (see, e.g., Ref. [38]), the drop is suspended from a tube. Creating instabilities by raising the potential of the tube is intermediate between the idealized situations described by (a) and (b). The stability conditions in experiments are usually discussed from the point of view [23] of increasing potential rather than charge. Therefore many features of the problem which are of interest to our study are usually not addressed. In Appendix B we summarize the relevant aspects from our perspective, while only quoting the main results in this section.

A closely related problem is that of an *insulating* uniformly charged drop. This problem has been considered in the framework of the charged drop model of atomic nuclei (see, e.g., Ref. [39]). The nonextensive portion of the energy of a spherical shape is now

$$E^{(i)}(Q) = \frac{3}{5}\frac{Q^2}{R} + 4\pi\gamma R^2 \ . \tag{12}$$

The similarity between Eqs. (11) and (12) is evident. As explained in Appendix B, this similarity persists even for the nonspherical shapes discussed in this section: all results for conducting drops are transformed into results for insulating drops by replacing $Q^2/2$ with $3Q^2/5$. This analogy, however, does not persist to arbitrary deformations and differences between conducting and insulating models will become apparent in Sec. V.

If the only allowed deformations of the charged drop are to ellipsoids of rotation (prolate spheroids), the spherical shape remains stable until α reaches 0.899. At this point the drop becomes strongly elongated with eccentricity $e = 0.95$, and continues to stretch with increasing α. For large α the long axis of the drop (and hence R_g) is proportional to $\alpha^{1/3}$. Due to the sharp increase in the aspect ratio of the spheroid with increasing α, the increase in the energy of the system slows down and becomes of the order of $(\alpha \ln \alpha)^{1/3}$ (compared to order of α for the undistorted sphere). Figure 7 depicts the resulting dependences of R_g^2 and E on α. The behavior of R_g^2 in Fig. 7 closely resembles the sudden expansion of polyamphilic gels in Ref. [7].

A more quantitative comparison between our results and the predictions of the charged drop model is possible: The transition in Fig. 5 appears at $\alpha' \equiv Q^2/(q_0^2 N) \approx 1$.

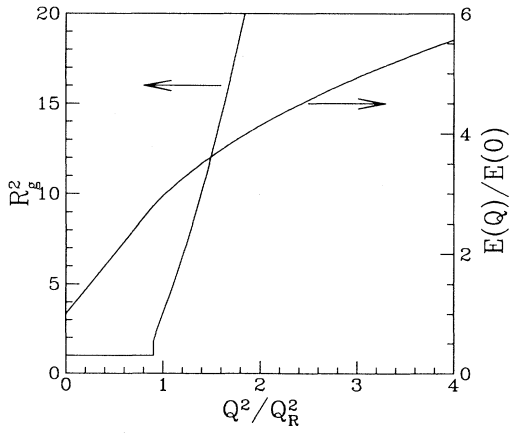

FIG. 7. Radius of gyration of the minimal energy spheroid in units of the radius of gyration of the undistorted sphere (left), and the energy of the spheroid scaled to that of the uncharged sphere (right), as a function of α.

The instability of a charged drop to ellipsoidal shape occurs for $\alpha \approx 0.9$ in the conducting case, and $\alpha \approx 0.7$ in the uniformly charged case. In Eq. (B1) we show that $\alpha = Q^2/(12V\gamma)$, where $V = a^3N$ is the volume of the system, while $\gamma \approx 0.1q_0^2/a^3$ [21]. Thus $\alpha \approx \alpha'$, and the observed critical value of α' is surprisingly close to the predictions of the model. (Given the numerous approximations of the model, such excellent agreement is probably fortuitous.) We conclude that, as long as the value of α is not too large, our Monte Carlo (MC) results, the predictions of the spheroidal drop model, and experiments, are in good agreement.

For comparison with Fig. 7, Fig. 8 depicts the energy per monomer as a function of scaled excess charge, obtained from MC simulations. At $Q = 0$, the curves for different N's almost coincide. (Slight corrections of order $N^{-1/3}$ are present, but invisible at this scale.) For small Q, the energy per monomer increases as $Q^2/(RN) \sim Q^2/N^{4/3}$, as indicated by the straight dashed line in Fig. 8. For large charges, the energy increase slows down, indicating distorted PA's. Since distortions start for $Q^2/q_0^2N \approx 1$, in terms of variables used in Fig. 8 the departures of longer chains begin earlier.

The results of this section are not sensitive to the exact shape of the elongated drop. Any shape characterized by a long dimension $R_\parallel$ and a short dimension $R_\perp$ (such as major and minor semiaxes of an ellipsoid) reproduces the same answers qualitatively. The electrostatic energy is approximately $\sim Q^2/R_\parallel$, while surface energy grows as $\gamma R_\perp R_\parallel$. Their sum has to be minimized subject to the constraint of fixed volume, imposed by requiring $V \approx R_\perp^2 R_\parallel$. For example, Gutin and Shakhnovich [40] consider the more general case of $Q \sim N^\beta$. Minimizing the total energy for elongated shapes, they find $R_\parallel \sim N^{(4\beta-1)/3}$, and $R_\perp \sim N^{2(1-\beta)/3}$. Only a finite stretching is predicted for $\beta = 1/2$. [A directed version of this problem also exhibits a continuously varying exponent $\nu(\beta)$ [41].] Another recent study by Dobrynin and Rubinstein [42] relaxes the constant volume constraint and also reaches the conclusion that there is an onset of stretching for $\beta = 1/2$, although a completely stretched state is reached only for $\beta = 2/3$, when the Coulomb energy becomes extensive.

However, as we shall show in the following sections, the ground state of a charged drop *is not* a simple elongated shape for large values of α. Conducting drops can shed away excess charge, while insulating drops disintegrate in a process similar to nuclear fission. Related pathways are available to PA's.

V. BEYOND SINGLE DROPS

Linear stability analysis indicates that a spherical shape is *unstable* to a variety of perturbations [26]. Experiments show that a conducting drop disintegrates when the Rayleigh stability limit is exceeded. Nuclear fission demonstrates the corresponding instability of insulating drops. Appendix C presents several mechanisms by which conducting and insulating drops can decrease their energy. For example, we show that a conducting charged drop can get rid of its *entire* electrostatic energy by emitting an infinite number of infinitesimal droplets.

The mechanisms discussed in Appendix C rely on the breakup of the charged drop. Such routes are not available to the PA chain which must maintain its connectivity. Is the charged PA susceptible to similar instabilities despite its connectivity? Figure 9 depicts $R_g^2(T = 0.1q_0^2/a)/R_g^2(T = \infty)$ as the function of the reduced charge $Q/N^{1/2}$ for different values of N. The curves become steeper with increasing N and intersect at $Q/N^{1/2} \approx 1.4q_0$. At the intersection point the radii scale as self-avoiding walks with a prefactor slightly larger than the infinite temperature value. For $Q > 1.4Q_c$ the PA's at low T are more stretched than self-avoiding walks, in disagreement with the finite elongation predicted for ellipsoidal shapes. How does the PA go beyond the ellipsoidal limit while maintaining its connectivity? We can still exploit analogies to charged drops.

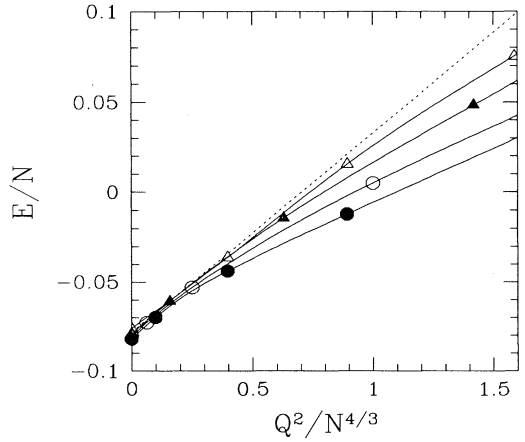

FIG. 8. Energy per monomer in units of q_0^2/a versus scaled excess charge for several chain lengths at $T = 0.05q_0^2/a$. The symbols are the same as in Fig. 5. The dashed line is the energy of an undistorted PA.

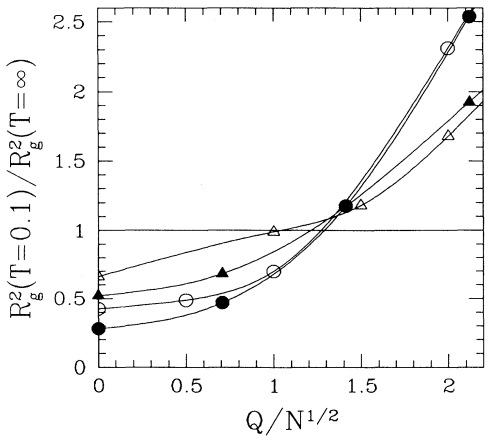

FIG. 9. Ratio between squared radii of gyration at $T = 0.1q_0^2/a$ and $T = \infty$ as a function of scaled excess charge. The symbols are the same as in Fig. 5.

The *annealed* PA is modeled by a deformable *conducting* "drop" of particles of size a, constrained to maintain a spherical topology. Although such a drop cannot expel charged particles, it can still reduce its energy by extruding charge in a finger of length L and diameter a. Due to the long-range nature of the Coulomb interactions in three dimensions, the electrostatic energy of an elongated object (of finite cross section) is determined only by its longest dimension. Balancing the Coulomb energy (Q^2/L) of the finger with the increase of surface energy γaL, we find that the optimal finger length is $L \approx Q/\sqrt{\gamma a}$. Fingers appear spontaneously only if their cost (roughly $Q\sqrt{\gamma a}$) is less than the Coulomb energy of the uniformly charged sphere, Q^2/R, i.e., for $Q > R\sqrt{\gamma a}$. The fingering instability occurs for $\alpha \approx a/R \ll 1$, i.e., far below the shape instability of a sphere. Thus the typical annealed PA has a protruding finger of length $L \propto Q \propto N^\beta$ for $\beta > 1/3$. But, as the weight of the finger is small, and it does not affect the scaling of R_g^2 for $\beta < 5/9$. Such PA's have large spanning sizes without appreciably greater R_g.

The *insulating* (uniformly charged) drop follows a different route. As is shown in Appendix C, it is stable for small α, but reduces its energy by splitting into several droplets of equal size for $\alpha > 0.293$. We can again constrain the overall object to remain singly connected by linking the droplets via narrow tubes of total length L and diameter a. As long as $La^2 \ll R^3$, most of the charge remains in the spheres. The total electrostatic energy is proportional to Q^2/L, while the surface energy cost grows as γaL. Equating the two gives $L \propto Q$; not surprisingly, of the same order as the fingers in the conducting case. However, whereas the surface tension in the conducting case results in one big central drop, for the insulating case the droplets are separated as in a *necklace*. The radius of gyration is now of the same order as the span of the necklace, L.

VI. RANDOMNESS IN THE NECKLACE MODEL

The necklace model provides a good picture of a polymer with a short-range attraction between its monomers and a *uniformly* distributed excess charge: A polymer with $Q \gg Q_R$ is split into roughly $\alpha \propto Q^2/N$ beads connected by a string. Each bead is just below the Rayleigh threshold, and the string is stretched by their Coulomb repulsion to a length $L \propto Q$. [Note that, as shown in Appendix C, the optimal number of beads is proportional to $(Q/Q_R)^2$ and not Q/Q_R.] For $Q \ll q_0 N$, only an infinitesimal fraction of monomers are part of the string, and the overall extensive part of the energy is unchanged. This picture should extend to any deterministic sequence, e.g., composed of alternating charges [17], which has a compact state when uncharged. It should be stressed that the reasoning that leads to the necklace model is somewhat speculative. The starting point is the continuum description of a globule, while the end result contains elements which rely on the discreteness of the monomers, where the continuum desciption is no longer valid. Further numerical work is required to confirm (or disprove) this picture.

Is the necklace model also applicable in the presence of random charges? For our model PA's $\alpha \approx Q^2/(q_0^2 N)$, with a prefactor almost identical to unity, and we shall use this relation as an exact definition of α. For $\alpha \gg 1$ we may try to split a chain into α segments of approximately equal size. Each segment has average charge $Q/\alpha \propto N/Q$ and incorporates $N/\alpha \propto (N/Q)^2$ monomers. Thus the fluctuations in charge of each segment are of the order of the average charge itself, and the picture of uniform, mutually repelling, beads is no longer applicable. It is not clear how we should model the shapes and distribution of the segments which have α's of order one.

Let us illustrate the difficulties caused by randomness for the case of an unrestricted PA. Since $\overline{Q^2} = q_0^2 N$, where the overline denotes an average over the ensemble of all quenches, we have $\overline{\alpha} = 1$. As demonstrated in Appendix C, the insulating drop is unstable to splitting already for $\alpha \approx 0.3$, and thus a typical random PA is expected to form several globules connected by narrow tubes. Now consider splitting sequences of N monomers with total charge constrained to a particular α into two equal subchains of charges Q_1 and Q_2. It is easy to show that each segment has $\overline{\alpha_{\text{subchain}}} = (1+\alpha)/2$, while the mean product of the charges is $\overline{Q_1 Q_2} = q_0^2 N(\alpha - 1)/4$. The subchains have, on average, values of α close to unity. Also, for $\alpha = 1$, the average value of the product of charges vanishes. We thus have the paradoxical situation in which most spherical shapes are unstable, while there is on average no energetic gain in splitting the sphere into two parts. It is most likely that the ensemble of chains with $\alpha \approx 1$ contains a broad distribution of sizes and shapes.

Thus charge inhomogeneities drastically modify the necklace picture. The resulting PA is probably still composed of rather compact globules connected by a (not necessarily linear) network of tubes. The globules are selected preferentially from segments of the chain that are approximately neutral (or at least below the instability threshold), while the tubes are from subsequences with larger than average excess charge. It is amusing to inquire how a random sequence is best partitioned into large neutral segments. The resulting segments appear to have a broad distribution which will be addressed in a future publication [21]. Some aspects of the distribution of large neutral segments in random sequences have been investigated by Kantor and Ertaş [43].

In summary, we find that the behavior of PA's and other charged polymers is controlled by the parameter $\alpha \propto Q^2/N$. Chains with small values of α form compact spherical globules. The globules split for $\alpha > 0.3$, resulting in a necklace of beads if the charge inhomogeneity is small. The span of the uniform necklace scales with the net charge Q. We do not have a consistent theoretical picture for the random PA beyond the instability threshold. The numerical results in Fig. 9 suggest that the size of such PA's grows faster than that of a self-avoiding walk, i.e., $\nu > 0.6$. The simulations so far are not inconsistent with $\nu = 1$ suggested by a scaling argument [10]. However, as the simulations suffer from the usual shortcomings of small sizes, sampling, and equili-

bration, a definitive answer about the behavior of PA's is still lacking.

ACKNOWLEDGMENTS

We would like to thank B.I. Halperin for bringing the importance of surface tension to our attention, and D. Ertaş for helpful discussions. This work was supported by the U.S.-Israel BSF Grant No. 92-00026, by the NSF through Grants No. DMR-87-19217 (at MIT's CMSE), No. DMR 91-15491 (at Harvard), and the PYI program (M.K.).

APPENDIX A: MONTE CARLO PROCEDURE

The model used for MC simulations is described in Sec. III. Discretizing monomer locations simplifies checking for excluded-volume interactions; allowing the bond length between the nearest neighbors to fluctuate without energetic cost (a "square-well" potential) provides sufficient flexibility to facilitate equilibration. The square-well potential has been used before in continuum simulations of tethered surfaces [44]; on discrete lattices it is known as the fluctuating bond method [45]. The details of the MC procedure are as follows.

For each T and Q we start by selecting a (quenched) random sequence of charges $\pm q_0$, whose sum (the total excess charge) is fixed to Q. This is accomplished by randomly selecting $(N - Q/q_0)/2$ positions on the chain for negative charges, and placing positive charges on the remainder. For each quench, we perform a thermal equilibration at temperature T, and then calculate the thermal averages of interest. The thermalization is repeated for ten different sequences and the results are averaged over the quenches. In an elementary MC step a monomer is picked at random and moved a single lattice unit. The move is accepted according to the usual Metropolis rule. Since each move requires recalculation of interaction energies, it involves $O(N)$ operations. The MC time unit is defined as the period during which N attempts are made. Thus the computer CPU time per single MC time unit increases as N^2.

Obtaining good averages in random systems is a significant challenge. Errors appear due to both inadequate thermal equilibration and insufficient quench averaging. Our high-temperature chains (for $T > 5q_0^2/a$) are similar to uncharged polymers and their equilibration is limited by the slowly decaying "Rouse modes." The slowest decay time is approximately the interval taken by a polymer to diffuse its own radius of gyration, estimated as follows: Since the acceptance rate of an elementary MC move is of order one throughout the simulation, the diffusion constant of a single monomer is also of order one (in units of squared lattice constant divided by the MC time unit). The diffusivity of the polymer center of mass is N times slower, resulting in a diffusion constant of $D \approx a^2/N$, and a relaxation time of $\tau' = R_g^2 N/a^2$. At high temperatures τ' scales as $N^{1+2\nu}$, where $\nu = 0.588$. At low temperatures ($T < 0.1q_0^2/a$) the polymer is almost compact, and a characteristic time can be obtained by considering phonons, plasma oscillations, or large-scale density fluctuations. Such time scales, in our MC time units, grow as $\tau'' \approx R_g^2/a^2 \sim N^{2/3}$. Unfortunately, there are probably much slower (and more important) time scales associated with crossing over large barriers to shape rearrangement which are thermally activated. We have no estimates for such times.

We used $\tau \equiv N^2$ MC units as the basic equilibration time. Each equilibration lasted 250τ, but the first 10τ configurations were dismissed in calculating thermal averages. As the number of operations per equilibration increases as N^4, this is close to the maximal equilibration time which can be reasonably used in a simulation of this type. Several hours of CPU time (on a Silicon Graphics R4000 computer workstation) were needed to equilibrate each quench at a given temperature for $N = 64$. Consequently, more than a day of CPU time is used to generate a single data point by averaging over ten quenches. To collect all the data on $N = 64$ chains we needed about two months of CPU. For $N = 128$ we spent ten days of CPU time to obtain a single data point, and therefore only the Q dependence at a single temperature was investigated.

We believe that the times used in equilibration produce satisfactory thermal averages. A direct check of the temporal correlation function of the radius of gyration for $N = 64$ indeed indicates that the correlation time is approximately equal to τ at high temperatures. This suffices to produce very good thermal averages. For example, a particular sequence of $N = 64$ monomers with $Q = 0$ at $T = 25$ has average $R_g^2 = 152a^2$, with standard deviation of approximately $60a^2$. For this polymer $\tau' = 152 \times 64 = 2.5\tau$, and thus our simulation contains approximately 100 independent configurations. Therefore the average value of R_g^2 is accurate to about $\pm 6a^2$. However, the average R_g^2 for ten distinct quenches are scattered over an interval of width $40a^2$. Thus the accuracy of our thermal averaging suffices to show that different quenches have slightly different thermal averages of R_g^2. The accuracy of the final average is, therefore, limited by the number of quenches rather than by the thermal averaging.

The correlation time obtained at low temperatures from temporal correlation functions of neutral PA's is shorter. This just reflects the reduction in size of the entire polymer. As mentioned earlier, correlations of R_g are rather insensitive to shape changes and their much longer activated time scales. To obtain some, admittedly indirect, measure of the quality of equilibration for dense polymers, we compare our simulations with the quite extensively investigated restricted primitive model (RPM). The latter represents a solution of positively and negatively charged particles ($\pm q_0$), interacting via a Coulomb force and a hard core repulsive potential of diameter σ. (For a review of the subject see Ref. [46].) The thermodynamics of the model is conveniently presented in terms of a dimensionless density $\rho_* \equiv n\sigma^3$ where n is the actual number density, and a dimensionless temperature $T_* \equiv k_B T\sigma/q_0^2$. At low temperatures the solution undergoes a phase separation between high and low density

phases. As indicated by the dashed line in Fig. 10, the critical point occurs at very low density (unlike regular fluids with short-range interactions). Numerical investigations of this phase transition [47–50] have encountered considerable difficulties: despite the low density, the behavior of the system becomes very erratic close to the critical point.

Since our simulations also involve low temperatures and relatively high densities, it is interesting to find out where our system is located on the (T_*, ρ_*) plane. Of course, as we are dealing with a single polymer rather than a dense solution, the comparison involves a few somewhat arbitrary factors. Our lattice potentials approximately mimic interactions of the hard core particles of RPM. From this comparison we relate the MC temperature to T_* by $T_* = 1.2Ta/q_0^2$. Second, we calculate the polymer density, assuming that the monomers uniformly occupy the volume of a homogeneous ellipsoid with identical eigenvalues of the shape tensor $\{\lambda_i\}$. This leads to a reduced density, $\rho_* = 2.4a^3/\sqrt{\lambda_1\lambda_2\lambda_3}$. For a neutral PA, ρ_* is approximately independent of T for $T > 5q_0^2/a$, and increases at lower T, leading to the trajectory indicated by the solid line in Fig. 10. At densities close to the critical density of RPM, the PA temperature is almost an order of magnitude higher than the critical temperature. At lower temperatures the trajectory of PA simulations approaches the phase boundary on the "liquid" side, at densities two times higher than the critical density of RPM. Thus our polymers stay away from the problematic region where critical fluctuations may cause significant equilibration problems. Since our equilibration times exceed by several orders of magnitude those used in RPM simulations, we believe that we have well equilibrated results.

The acceptance rate of MC moves in our simulations is approximately 0.6 for all temperatures. It drops to 0.46 at $T = 0.05q_0^2/a$, and further lowering of temperature leads to a gradual "freezing." Repeated heating and cooling cycles performed on several samples indicates that the behavior is essentially reversible for $T > 0.05q_0^2/a$. We believe that the configurations obtained for $T = 0.05q_0^2/a$ are very close to the actual ground state. Most of the low-temperature investigations were actually performed at $T = 0.1q_0^2/a$ where the thermal averages are more reliable. For chain length $N = 64$ we performed an extensive study of the dependence of R_g and other quantities on T and Q. We also investigated the N dependence of these quantities at $T = 0.1q_0^2/a$ for $N = 16$, 32, 64, and 128.

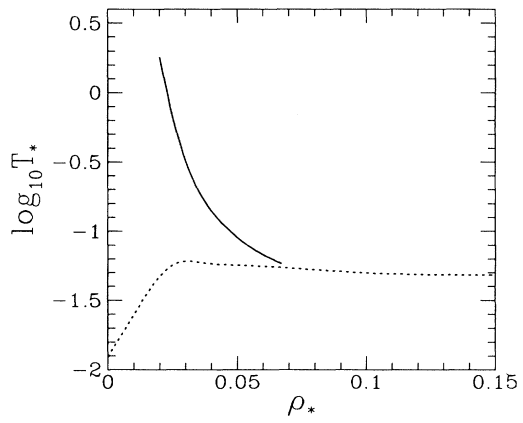

FIG. 10. High and low density fluid ("liquid" and "gas") transition line (dotted) in the plane, (T_*, ρ_*), where T_* and ρ_* are the reduced temperature and density (see text) of the restricted primitive model. The solid line indicates the trajectory of the neutral PA's used in our MC simulations.

APPENDIX B: SPHEROIDAL DISTORTIONS OF CHARGED DROPS

In this appendix we discuss the minimum energy shape of a single charged drop. We first examine the conducting drop, and then relate the results to insulating ones in the last paragraph. In terms of the dimensionless parameter α, Eq. (11) for the energy of a charged conducting spherical drop is

$$E(Q) = E(0)(1 + 2\alpha). \tag{B1}$$

For large Q the spherical shape is unstable, and the stable shape is determined by minimizing the sum of surface and electrostatic energies. In an equilibrium shape the surface is an equipotential, since otherwise energy can be reduced by redistributing the surface charge. The pressure difference between the inside and outside of the drop at any point on the surface is given by

$$\Delta p = \gamma\left(\frac{1}{r_1} + \frac{1}{r_2}\right) - 2\pi\sigma^2 , \tag{B2}$$

where r_1 and r_2 are the principal radii of curvature, and σ is the surface charge density. In equilibrium the pressure inside the drop must be constant. Thus Eq. (B2), with a constant value of Δp at all points, determines the equilibrium shape. This is in fact a rather complicated integro-differential equation whose general solutions are not known. Note that for $Q = Q_R$, we find $\Delta p = 0$ for a spherical drop.

In 1882 Lord Rayleigh investigated the stability of a charged drop [22] and showed that for $\alpha = 1$ the sphere becomes unstable to surface distortions described by the Legendre function $P_2(\cos\theta)$. [The points of instability for higher harmonics are given by $\alpha_n = (n + 2)/4$.] The instability does not result in a small distortion as α exceeds unity but, rather, leads to a strongly elongated shape. For $\alpha > 1$ no exact analytical treatment is available. Some progress is possible by assuming that the drop is an ellipsoid of revolution (i.e., a prolate spheroid) [23]. Since both the surface area and the electrostatic energy of such shapes are known (see, e.g., Ref. [51]), the problem reduces to the minimization of

$$E(Q) = \frac{E(0)}{2}\left[(1-e^2)^{1/3}\left(1 + \frac{\sin^{-1} e}{e\sqrt{1-e^2}}\right) + 2\alpha\frac{(1-e^2)^{1/3}}{e}\ln[(1+e)/(1-e)]\right], \tag{B3}$$

with respect to eccentricity $e \equiv \sqrt{1-b^2/a^2}$, where a and b are the major and minor semiaxes. The first term in the large square brackets is the total surface area (incorporating the constraint of fixed volume), while the second term is the electrostatic energy (Q enters via α). It has been shown [23] that a prolate spheroid is *not* an exact equilibrium shape: for aspect ratio $a:b=2:1$ the pressure difference Δp in Eq. (B2) varies by about 2% for different points on the surface. Nevertheless, we may assume that the forces pulling the ellipsoid out of the shape are small as long as a/b is not excessively large. Numerical solutions of a drop in an external field confirm that the ellipsoidal approximation is reasonably good for shapes that are not too elongated [29,34,33].

Ailam and Gallily [24] noted that Eq. (B3) has a local minimum for $e \neq 0$ even for α smaller than unity, i.e., below the Rayleigh stability limit. However, they did not determine this range accurately. Figure 11 depicts $E(Q)$ as a function of e for several values of α in the relevant parameter range. A new local minimum first appears for $\alpha = 0.887$, and becomes the *global* minimum for $\alpha > 0.899$. At the latter α a spherical drop should discontinuously "jump" to a strongly elongated shape with $e = 0.95$. However, the spherical shape ($e = 0$) remains a *local* minimum until $\alpha = 1$. In an ideal experiment in which the charge is gradually increased the drop stays in a metastable spherical shape. At $\alpha = 1$, the sphere becomes unstable and stretches to $e = 0.98$. For $\alpha \gg 1$, the eccentricity approaches unity. In this limit, the asymptotic forms of the surface and electrostatic energy are $(1-e)^{-1/6}$ and $-(1-e)^{1/3}\ln(1-e)$, respectively. The minimum energy is achieved at $e^2 \approx 1-(\pi/8\alpha)^2/\ln^2(\pi/8\alpha)^2$, while the energy increases as

$$E(Q) \approx 2.03E(0)(\alpha \ln \alpha)^{1/3} . \tag{B4}$$

Note that the asymptotic increase of $E(Q)$ ($\propto Q^{2/3}$) is much smaller than that of the undeformed sphere ($\propto Q^2$). The exact dependence of $E(Q)$ on α is plotted in Fig. 7. In the same figure we also present the squared radius of gyration of the elliptical drop,

$$\frac{R_g^2(Q)}{R_g^2(0)} = \frac{a^2+2b^2}{3R^2} = \frac{(1-e^2)^{-\frac{2}{3}}+2(1-e^2)^{\frac{1}{3}}}{3} . \tag{B5}$$

Since for large Q, $1-e^2$ is proportional to α^{-2} up to logarithmic terms, $R_g \sim R\alpha^{2/3} \sim R(Q/Q_R)^{4/3}$. While the ellipsoidal shape is not an exact solution to the charged drop problem, Eq. (B4) provides an upper bound on the total energy.

We next consider a drop in which the charge is *uniformly* distributed over the volume. This system has been considered in the context of the liquid drop model of atomic nuclei (see, e.g., Ref. [39]). The energy of the uniformly charged sphere, Eq. (12), is

$$E^{(i)}(Q) = E(0)\left(\frac{12}{5}\alpha+1\right) . \tag{B6}$$

As in the case of the conducting drop, the uniformly charged drop becomes locally unstable [52–54] to infinitesimal distortions for $\alpha = 5/6$. Assuming that the drop distorts into a prolate spheroid, its energy can be written down explicitly [54]. The resulting energy is identical to Eq. (B3), except that the factor of 2α in the second term is replaced by $12\alpha/5$. The same factor relates Eqs. (B1) and (B6). Thus all the previous results for conducting drops are also applicable to insulating drop after multiplying α's by 6/5. We should note that this simple substitution does not hold for drops of arbitrary shape.

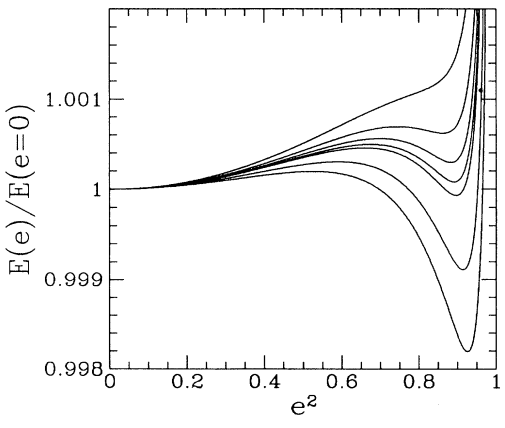

FIG. 11. Energy differences between drops of prolate spheroidal, and spherical, shape (normalized to the energy of spherical drop) as a function of squared eccentricity e^2. The graphs correspond (from top to bottom) to $\alpha = 0.88$, 0.89, 0.895, 0.898, 0.90, 0.91, and 0.92.

APPENDIX C: SPLITTING A CHARGED DROP

An elongated ellipse is not a *local* equilibrium shape of a drop, since perturbations $P_n(\cos\theta)$ with $n > 2$ become unstable [26]. There are other theoretical indications that no elongated shape is the *global* ground state. For example, as the eccentricity increases the electric field at a tip [$\sim Q/b^2 \sim Q(1-e^2)^{-1/3}$] becomes strong enough to support conical tips [23,33]. Experimentally, it is observed that, for $\alpha > 1$, a conducting charged drop disintegrates into smaller ones. Assuming that the experiments can be described by the charged drop model [38,55,56], disintegration begins for α equal to or slightly above one. This is not surprising, since already at $\alpha = 1$ the equilibrium shape is strongly deformed. The instabilities lead to ejection of smaller droplets whose size distribution is believed to be controlled by hydrodynamic effects. Apparently, after a significant elongation, many roads towards decreasing energy open up and the choice is made by dynamical effects. In this appendix we shall investigate the splittings of a drop into several spherical droplets removed to infinite separations.

First consider the splitting of a single *conducting* drop of radius R into two (secondary) droplets with radii R_1 and R_2. Using Eq. (B1) for the energy of each droplet,

the total energy of the infinitely separated pair is

$$E_2(Q) = \frac{q_1^2}{2R_1} + \frac{q_2^2}{2R_2} + 4\pi\gamma(R_1^2 + R_2^2) \ . \qquad \text{(C1)}$$

The charges satisfy $q_1 + q_2 = Q$, while the radii are constrained by $R_1^3 + R_2^3 = R^3$ to preserve the total volume. Minimizing $E_2(Q)$ with respect to q_1, while treating q_2 as a dependent variable, gives

$$q_i = \frac{R_i}{\sum_j R_j} Q. \qquad \text{(C2)}$$

Substituting this result into Eq. (C1) we find

$$E_2(Q) = E(0)\left(\frac{2\alpha}{\sum_j r_j} + \sum_j r_j^2\right) \ , \qquad \text{(C3)}$$

where the reduced radii $r_j \equiv R_j/R$ satisfy the fixed volume constraint $\sum_j r_j^3 = 1$. [Note that $E(0)$ denotes the surface energy of the *original* drop.] The stationary value of $E_2(Q)$ is found by solving $\partial E_2(Q)/\partial r_1 = 0$, and treating r_2 as a dependent variable. The resulting equation has several possible solutions, including

$$r_1^3 = r_2^3 = \frac{1}{2}. \qquad \text{(C4)}$$

However, the symmetrical solution is a *minimum* only for $\alpha \geq 1$. Thus strongly charged drops would prefer splitting into two equal droplets. A second solution,

$$r_{1,2}^3 = \frac{1}{2}\left(1 \pm \sqrt{1 - \frac{4\alpha^3}{1+3\alpha}}\right), \qquad \text{(C5)}$$

exists only for $\alpha \leq 1$, where it is an energy minimum, less than that of a single sphere. Thus a weakly charged drop can always reduce its energy by splitting into two unequal parts.

Further breakup of the drop is possible, and we next consider splittings into n droplets. The solution to this problem is analogous to the previous case. The distribution of charge among the droplets is still given by Eq. (C2) and $E_n(Q)$ has exactly the same form as Eq. (C3) with j summed from 1 to n. The search for extrema of $E_n(Q)$ leads to several solutions, classified by two sets of droplets. One set contains m small droplets of reduced radius a, while the remaining $m-n$ have larger reduced radii b ($b > a$), such that

$$ma^3 + (n-m)b^3 = 1 \ , \qquad \text{(C6)}$$

$$a = \frac{\alpha b}{b\,[ma + (n-m)b]^2 - \alpha} \ .$$

The solution for a particular m exists only in a finite range of α's, and finding which solution represents the global energy minimum is quite cumbersome. One limit, however, is easily examined: Consider splitting the drop into one large droplet and $m = n-1$ smaller drops. In the limit of $n \to \infty$, $a^3 \approx \alpha/n^2$, and $b \approx 1$; the total volume, area, and electrostatic energy of the charged droplets, vanishes, while they, nevertheless, carry all the charge of the system. Thus the energy of the system is reduced to $E(0)$, i.e., the energy of the uncharged original drop.

We next consider the insulating *uniformly charged* drop. If such a drop is split in two, the charge of each droplet will be proportional to its volume, i.e., $q_i = QR_i^3/R^3$. Using the energy of a single sphere in Eq. (B6), the total energy of a pair of infinitely separated spherical droplets is obtained as

$$E_2^{(i)}(Q) = \frac{3}{5}\sum_j \frac{q_j^2}{R_j} + 4\pi\gamma \sum_j R_j^2$$
$$= E(0)\left[\frac{12}{5}\alpha \sum_j r_j^5 + \sum_j r_j^2\right] \ . \qquad \text{(C7)}$$

The charges $\{q_j\}$ and the reduced radii $\{r_j\}$ satisfy the same restrictions as in the conducting drop. For $\alpha < 1/6$ the only extremum is a maximum at $r_1^3 = r_2^3 = 1/2$. For $\alpha > 1/6$, this point is a local minimum. However, only for $\alpha > 0.293$ is the resulting energy lower than that of the original drop. A similar scenario is found for splitting the drop into n secondary droplets. Larger values of α are needed to stabilize solutions with higher n, and there is an optimal number of droplets (all of the same radius) for each α. Since the energy of an n-drop system is

$$E_n^{(i)} = n\left[\frac{3}{5}\left(\frac{Q}{n}\right)^2\left(\frac{n}{R^3}\right)^{1/3} + 4\pi\gamma\left(\frac{R^3}{n}\right)^{2/3}\right]$$
$$= E(0)\left[\frac{12}{5}\alpha n^{-2/3} + n^{1/3}\right] \ , \qquad \text{(C8)}$$

the optimal n (for large n) is found from $\partial E_n^{(i)}/\partial n = 0$ as

$$n = \frac{24}{5}\alpha \ . \qquad \text{(C9)}$$

The total energy of the optimal configuration grows as

$$E_{\text{optimal}}^{(i)}(Q) = 2.53E(0)\alpha^{1/3}. \qquad \text{(C10)}$$

Thus the uniformly charged drop cannot lower its energy as drastically as its conducting counterpart. Since we have not exhaustively searched for other configurations, the above result should be regarded as an upper bound to the ground state energy. Note that this bound has the same scaling (up to logarithmic corrections) on α as that of the highly elongated spheroid.

[1] C. Tanford, *Physical Chemistry of Macromolecules* (Wiley, New York, 1961).
[2] See, e.g., T.E. Creighton, *Proteins: Their Structure and Molecular Properties* (Freeman, San Francisco, 1984).
[3] D.L. Stein, Proc. Natl. Acad. Sci. USA **82**, 3670 (1985); J.D. Bryngelson and P.G. Wolynes, *ibid.* **84**, 7524 (1987); H.S. Chan and K.A. Dill, Phys. Today **46**(2), 24 (1993).
[4] T. Garel and H. Orland, Europhys. Lett. **6**, 307 (1988); E.I. Shakhnovich and A.M. Gutin, *ibid.* **8**, 327 (1989); M. Karplus and E.I. Shakhnovich, in *Protein Folding*, edited by T. E. Creighton (Freeman & Co., New York, 1992), Chap. 4, p. 127.
[5] M. Mézard, G. Parisi, and M.A. Virasoro, *Spin Glass Theory and Beyond* (World Scientific, Singapore, 1987).
[6] M. Scouri, J.P. Munch, S.F. Candau, S. Neyret, and F. Candau, Macromolecules **27**, 69 (1994).
[7] X.-H. Yu, A. Tanaka, K. Tanaka, and T. Tanaka, J. Chem. Phys. **97**, 7805 (1992); X.-H. Yu, Ph.D. thesis, MIT, 1993.
[8] M. Annaka and T. Tanaka, Nature (London) **355**, 430 (1992).
[9] P. Pfeuty, R.M. Velasco, and P.G. de Gennes, J. Phys. (Paris) Lett. **38**, L5 (1977).
[10] Y. Kantor and M. Kardar, Europhys. Lett. **14**, 421 (1991).
[11] L.D. Landau and E.M. Lifshitz, *Statistical Physics* (Pergamon, New York, 1981), Pt. 1.
[12] P.G. Higgs and J.-F. Joanny, J. Chem. Phys. **94**, 1543 (1991).
[13] Y. Kantor, H. Li, and M. Kardar, Phys. Rev. Lett. **69**, 61 (1992).
[14] Y. Kantor, M. Kardar, and H. Li, Phys. Rev. E **49**, 1383 (1994).
[15] Y. Kantor and M. Kardar, Europhys. Lett. **27**, 643 (1994).
[16] J. Wittmer, A. Johner, and J.F. Joanny, Europhys. Lett. **24**, 263 (1993).
[17] J.M. Victor and J.B. Imbert, Europhys. Lett. **24**, 189 (1993).
[18] E. Raphael and J.F. Joanny, Europhys. Lett. **13**, 623 (1990).
[19] S.F. Edwards, P.R. King, and P. Pincus, Ferroelectrics **30**, 3 (1980).
[20] P.G. de Gennes, *Scaling Concepts in Polymer Physics* (Cornell University Press, Ithaca, 1979).
[21] Y. Kantor and M. Kardar (unpublished).
[22] Lord Rayleigh, Philos. Mag. **14**, 184 (1882).
[23] G. Taylor, Proc. R. Soc. London, Ser. A **280**, 383 (1964).
[24] G. Ailam (Volinez) and I. Gallily, Phys. Fluids **5**, 575 (1962).
[25] C.D. Hendricks and J.M. Schneider, Am. J. Phys. **16**, 450 (1963).
[26] A.I. Grigor'ev, Zh. Tekh. Fiz. **55**, 1272 (1985) [Sov. Phys. Tech. Phys. **30**, 736 (1985)].
[27] A.I. Grigor'ev and S.O. Shiryaeva, Zh. Tekh. Fiz. **61**, 19 (1991) [Sov. Phys. Tech. Phys. **36**, 258 (1991)].
[28] S.O. Shiryaeva and A.I. Grigor'ev, Zh. Tekh. Fiz. **62**, 35 (1992) [Sov. Phys. Tech. Phys. **37**, 254 (1992)].
[29] M.J. Miksis, Phys. Fluids **24**, 1967 (1981).
[30] J.D. Sherwood, J. Fluid Mech. **188**, 133 (1988).
[31] P.R. Brazier-Smith, Phys. Fluids **14**, 1 (1971).
[32] J.C. Bacri and D. Salin, J. Phys. (Paris) Lett. **43**, 649 (1982).
[33] H. Li, T.C. Halsey, and A. Lobkovsky, Europhys. Lett. **27**, 575 (1994).
[34] O.E. Sero-Guillaume, D. Zouaoui, D. Bernadin, and J. P. Brancher, J. Fluid Mech. **241**, 215 (1992).
[35] J.C. Bacri, D. Salin, and R. Massarat, J. Phys. (Paris) Lett. **43**, L179 (1982).
[36] W.H. Liao and D.A. Krueger, J. Colloid. Interface Sci. **70**, 564 (1979).
[37] C.G. Hayes, J. Colloid. Interface Sci. **52**, 239 (1975).
[38] J. Zeleny, Phys. Rev. **10**, 1 (1917).
[39] J.M. Blatt and V.F. Weisskopf, *Theoretical Nuclear Physics* (Wiley, New York, 1952), Chap. 7, p. 303; R.D. Evans, *The Atomic Nucleus* (McGraw-Hill, New York, 1955), Chap. 11, p. 387.
[40] A.M. Gutin and E.I. Shakhnovich (unpublished).
[41] B. Derrida and P.G. Higgs, in *Surface Disordering, Growth, Roughening and Phase Transitions*, Les Houches, edited by R. Jullien, J. Kertesz, P. Meakin, and D. E. Wolf (Nova Science, New York, 1993).
[42] A.V. Dobrynin and M. Rubinstein (unpublished).
[43] Y. Kantor and D. Ertaş, J. Phys. A (to be published).
[44] Y. Kantor, M. Kardar, and D.R. Nelson, Phys. Rev. Lett. **57**, 791 (1986).
[45] I. Carmesin and K. Kremer, Macromolecules **21**, 2819 (1988).
[46] M.E. Fisher, J. Stat. Mech. **75**, 1 (1994).
[47] M.E. Fisher and Y. Levin, Phys. Rev. Lett. **71**, 3826 (1993).
[48] H.L. Friedman, J. Chem. Phys. **70**, 92 (1979).
[49] J.P. Valleau, J. Chem. Phys. **95**, 584 (1991).
[50] A.Z. Panagiotopoulos, Fluid Phase Equil. **76**, 97 (1992).
[51] J.H. Jeans, *Electricity and Magnetism* (Cambridge University Press, Cambridge, England, 1948), p. 244.
[52] N. Bohr and J.A. Wheeler, Phys. Rev. **56**, 426 (1939).
[53] E. Feenberg, Phys. Rev. **55**, 504 (1939).
[54] F. Weizsäcker, Naturwissenschaften **27**, 133 (1939).
[55] H.M.A. Elghazaly and G.S.P. Castle, IEEE Trans. Ind. Appl. **25**, 48 (1989).
[56] S.A. Ryce and D.A. Patriarche, Can. J. Phys. **43**, 2192 (1965).